J Biomol NMR (2009) 45:45–55
DOI 10.1007/s10858-009-9310-6

ARTICLE

CPMG relaxation dispersion NMR experiments measuring glycine $^{1}H^{\alpha}$ and $^{13}C^{\alpha}$ chemical shifts in the 'invisible' excited states of proteins

Pramodh Vallurupalli · D. Flemming Hansen · Patrik Lundström · Lewis E. Kay

Received: 12 January 2009 / Accepted: 26 February 2009 / Published online: 25 March 2009

Abstract Carr-Purcell-Meiboom-Gill (CPMG) relaxation dispersion NMR experiments are extremely powerful for characterizing millisecond time-scale conformational exchange processes in biomolecules. A large number of such CPMG experiments have now emerged for measuring protein backbone chemical shifts of sparsely populated (>0.5%), excited state conformers that cannot be directly detected in NMR spectra and that are invisible to most other biophysical methods as well. A notable deficiency is, however, the absence of CPMG experiments for measurement of $^{1}H^{\alpha}$ and $^{13}C^{\alpha}$ chemical shifts of glycine residues in the excited state that reflects the fact that in this case the $^{1}H^{\alpha}$, $^{13}C^{\alpha}$ spins form a three-spin system that is more complex than the AX $^{1}H^{\alpha}$–$^{13}C^{\alpha}$ spin systems in the other amino acids. Here pulse sequences for recording $^{1}H^{\alpha}$ and $^{13}C^{\alpha}$ CPMG relaxation dispersion profiles derived from glycine residues are presented that provide information from which $^{1}H^{\alpha}$, $^{13}C^{\alpha}$ chemical shifts can be obtained. The utility of these experiments is demonstrated by an application to a mutant of T4 lysozyme that undergoes a millisecond time-scale exchange process facilitating the binding of hydrophobic ligands to an internal cavity in the protein.

Keywords CPMG · Relaxation dispersion · Excited protein states · T4 lysozyme · Millisecond dynamics

Electronic supplementary material The online version of this article (doi:10.1007/s10858-009-9310-6) contains supplementary material, which is available to authorized users.

P. Vallurupalli · D. F. Hansen · P. Lundström · L. E. Kay (✉)
Departments of Molecular Genetics, Biochemistry and Chemistry, University of Toronto, Toronto, ON M5S 1A8, Canada
e-mail: kay@pound.med.utoronto.ca

Introduction

The conformations of biological molecules are not static but rather fluctuate over a wide range of timescales (Austin et al. 1975; Karplus 2000). Such fluctuations are often critical for function by influencing both the kinetics and the thermodynamics of the processes in which these molecules participate (Karplus and Kuriyan 2005). It is therefore of considerable interest to characterize such dynamics in detail as a means of providing insight into how molecular function proceeds. NMR spectroscopy has emerged as a powerful tool for studying motion over a broad range of time-scales, from picoseconds to seconds, (Mittermaier and Kay 2006; Palmer 2004) and in the past years a large number of experiments have been developed that extend the scope of the methodology to include ever more complex biological systems. A particularly important class of experiment is the Carr-Purcell-Meiboom-Gill (CPMG) relaxation dispersion method (Carr and Purcell 1954; Meiboom and Gill 1958), originally developed close to 50 years ago, that has been extensively modified for applications to biomolecules (Loria et al. 1999; Palmer et al. 2001). In CPMG measurements the effective transverse relaxation rates, $R_{2,\mathrm{eff}}$, of probes such as ^{15}N, ^{1}H or ^{13}C nuclei are monitored as a function of the frequency, ν_{CPMG}, at which refocusing π pulses are applied during a relaxation delay. Modulation of the chemical shifts of these probes due to a conformational exchange process, leads to a dependence of $R_{2,\mathrm{eff}}$ on ν_{CPMG} because the π pulses refocus chemical shift evolution, quenching the effects of chemical exchange. In the case of a two-site exchange process, $A \underset{k_{BA}}{\overset{k_{AB}}{\rightleftharpoons}} B$, the $R_{2,\mathrm{eff}}$ versus ν_{CPMG} profile (relaxation–dispersion curve) depends on the population of the minor state, p_B, the rate of exchange between states,

$k_{ex} = k_{AB} + k_{BA}$ and the absolute value of the chemical shift difference, $|\Delta\varpi|$, between spins in the major and minor states (Palmer et al. 2001). The sign of $\Delta\varpi$ can, in turn, be obtained independently by comparing the position of the peaks in HSQC and HMQC data sets recorded at a number of static magnetic fields (Skrynnikov et al. 2002).

The attraction of the CPMG experiment is that it can provide detailed information about the kinetics and thermodynamics of conformational exchange processes between major (the ground state) and minor (excited state) conformers, so long as the latter are populated to greater than approximately 0.5% and the exchange process is on the millisecond timescale (Korzhnev and Kay 2008; Korzhnev et al. 2004; Palmer 2004). Because these minor states are often transiently formed and are of low population they are 'invisible' to many of the conventional structural biology tools. The CPMG method thus provides a window into studying these states that are recalcitrant to other techniques and applications to protein folding, enzyme catalysis and binding have emerged recently (Boehr et al. 2006; Grey et al. 2006; Henzler-Wildman et al. 2007; Korzhnev et al. 2004; Sugase et al. 2007; Vallurupalli and Kay 2006; Watt et al. 2007).

In addition to characterizing the kinetics and thermodynamics of exchange processes involving excited states it is also possible to obtain structural information pertaining to these minor conformers. One source of this information is provided by the chemical shifts that are extracted from fits of relaxation dispersion measurements (Grey et al. 2003; Hansen et al. 2008c; Korzhnev et al. 2004; Vallurupalli et al. 2008b). Chemical shifts of nearly all sites along a protein backbone (^{1}HN, ^{15}N, $^{13}C^{\alpha}$, ^{13}CO and $^1H^{\alpha}$) in the 'invisible' excited state can be determined using recently developed CPMG experiments in concert with new labeling schemes (Hansen et al. 2008a, b, c, d; Lundstrom et al. 2009). Complementary information is provided in the form of residual anisotropic interactions (residual dipolar couplings, RDCs, and chemical shift anisotropies, RCSAs) that can now be measured for minor conformers using spin-state selective CPMG relaxation dispersion experiments (Hansen et al. 2008b; Igumenova et al. 2007; Vallurupalli et al. 2008a, 2007a). The combination of chemical shifts, RDCs and RCSAs has recently been used to determine the backbone fold of an invisible conformer corresponding to a ligand bound form of an SH3 domain (Vallurupalli et al. 2008b).

One residue for which excited state $^1H^{\alpha}$ and $^{13}C^{\alpha}$ chemical shifts are conspicuously absent is Gly. This is unfortunate since in general Gly residues can populate extensive regions of (Φ, Ψ) space (Ramakrishnan and Ramachandran 1965). Restraints on the backbone torsion angles of Gly, provided by $^1H^{\alpha}$, $^{13}C^{\alpha}$ chemical shifts, would thus be very valuable in structural studies. The difficulty in recording robust relaxation dispersion profiles of Gly stems from the fact that unlike other amino acids the $^1H^{\alpha}$, $^{13}C^{\alpha}$ spins of this residue form an AMX/ABX/AX_2 spin system. Measurement of Gly $^1H^{\alpha}$ shifts in the excited state is complicated by the two-bond $^1H^{\alpha}$–$^1H^{\alpha}$ homonuclear scalar coupling that renders transverse ^{1}H magnetization dependent on ν_{CPMG}, even in the absence of chemical exchange (Lundstrom et al. 2009). While ^{15}N CPMG pulse schemes have been published for NH_2 groups of Asn and Gln residues (Mulder et al. 2001b) that could be easily modified for ^{13}C studies of Gly, the rapid $^{13}C^{\alpha}$ transverse relaxation resulting from the pair of one-bond coupled protons decreases the sensitivity of the ^{13}C probe to chemical exchange processes. Here we address these problems by using a labeling scheme in which uniformly ^{13}C labeled proteins are enriched to approximately 50% ^{2}H at the α-position by expression in media that is 50% D_2O based and selecting for ^{13}CHD moieties in CPMG pulse schemes that measure Gly $^1H^{\alpha}$ and $^{13}C^{\alpha}$ dispersion profiles. The methodology is applied to a cavity mutant of T4 lysozyme (18.8 kDa) in which Leu at position 99 is replaced by Ala (referred to in what follows as T4 L99A) (Eriksson et al. 1992). T4 L99A is able to bind hydrophobic ligands on the millisecond time-scale (Feher et al. 1996) through an exchange mechanism involving interconversion between a highly populated (and ligand inaccessible) ground state and a binding competent excited state that is amenable to characterization by CPMG relaxation dispersion (Mulder et al. 2000, 2001a). Here we show that some of the $^1H^{\alpha}$ and $^{13}C^{\alpha}$ spins of the 11 Gly probes in the protein are sensitive to this exchange event.

Materials and methods

Protein expression and purification

100% ^{13}C, >50% ^{2}H enriched samples of T4 lysozyme with the cavity forming mutation L99A were prepared by expressing protein in *E coli* BL21(DE3) cells. Cells were grown in one liter of 50% D_2O, M9 media supplemented with 1 g $^{15}NH_4Cl$ and 3 g [$^{13}C_6$, $^2H_7$]-glucose as the nitrogen and carbon sources, respectively. The cells were grown to an OD_{600} of 0.8 at 37°C, with the temperature reduced to 18°C for protein expression induced with 1 mM IPTG. After expression for 16 h the cells were harvested by centrifugation. The cell pellet was suspended in 50 mM sodium phosphate, 2 mM EDTA, pH 6.5 and lysed by sonication. The lysate was then loaded on a 5 mL HiTrap SP Sepharose column (GE Healthcare) that binds the protein, with elution achieved by increasing the salt concentration linearly to 1 M NaCl in the same buffer as described above. Fractions containing the protein (as determined by UV absorption and PAGE) were pooled together and concentrated to 1 mL. The

protein was further purified by gel filtration using a 120 mL Superdex 75 column (GE Healthcare) equilibrated with 50 mM sodium phosphate, 100 mM NaCl, 2 mM EDTA pH 5.5. Fractions containing the pure protein were pooled together and transferred into 100% D_2O NMR buffer comprised of 50 mM sodium phosphate, 25 mM NaCl, 2 mM EDTA, 2 mM NaN_3 pH 5.5. The final 500 μL NMR sample was at a concentration of 1.4 mM.

In order to test ^2H decoupling in the Gly-$^{13}C^{\alpha}$ CPMG pulse scheme that is presented below we have chosen a smaller protein system from which spectra of high signal to noise can be obtained. A 1 mM sample of the Abp1p SH3 domain (~7 kDa) in 50 mM sodium phosphate, 100 mM NaCl, 2 mM EDTA, 2 mM NaN_3, pH 7.0 buffer, 100% D_2O, labeled as described above for T4 L99A was produced as described previously (Lundstrom et al. 2009).

NMR spectroscopy

All NMR experiments were performed at 25°C using 600 and 800 MHz Varian Inova spectrometers equipped with cryogenically cooled (600) and room temperature (800) triple resonance probes. $^1H^{\alpha}$ CPMG experiments (Fig. 1) were recorded with a constant time CPMG delay, T_{relax}, of 16 (15) ms at 600 (800) MHz. Data were recorded for 14 (15) ν_{CPMG} values ranging from 62.5 (133) to 1250 (1867) Hz with 2 (3) repeat measurements at 600 (800) MHz. Here $\nu_{CPMG} = 1/(4\tau_{CP})$, where $2\tau_{CP}$ is the time between refocusing π pulses during the CPMG pulse train. Experiments were recorded with acquisition times of (24, 64 ms) in (t_1, t_2), with 64 (32) transients per FID and with a delay of 2.5 s between transients giving rise to a total acquisition time for each full dispersion set of 42 (22) h at 600 (800) MHz. $^{13}C^{\alpha}$ CPMG dispersion profiles were measured at 600 MHz using the pulse scheme described in the text with $T_{relax} = 14$ ms. Thirteen ν_{CPMG} values ranging from 71 to 930 Hz were obtained with three repeat measurements for error estimation. Forty-eight transients were recorded for each point in the indirect dimension with a recycle delay of 2.5 s leading to a total experimental time of 42 h. Acquisition times in (t_1, t_2) were (24, 64 ms) as before.

Data analysis

Spectra were processed using nmrPipe (Delaglio et al. 1995), visualized with Sparky (Goddard and Kneller), with

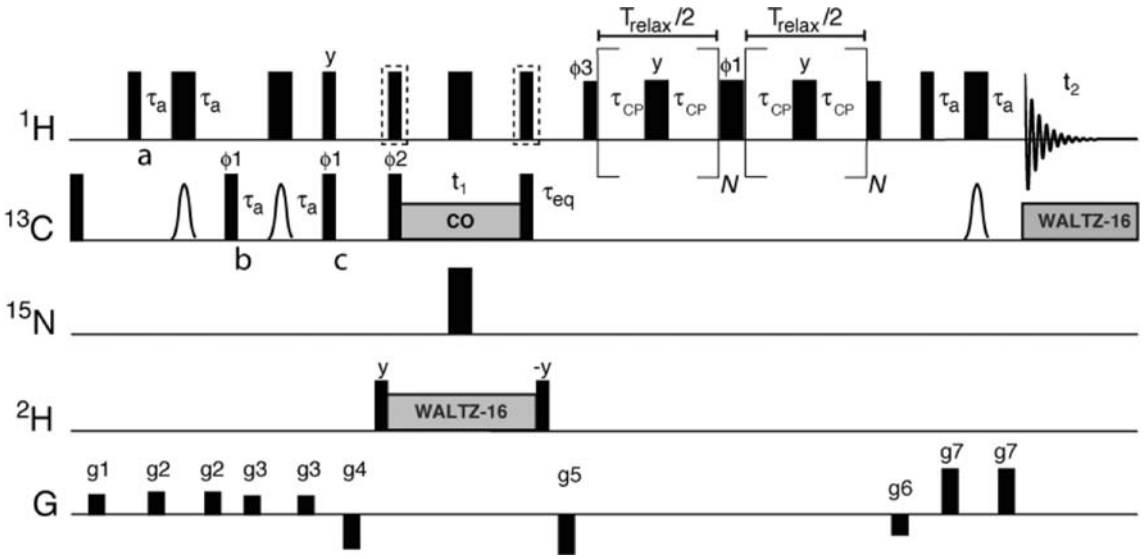

Fig. 1 Pulse sequence for recording $^1H^{\alpha}$ CPMG relaxation dispersion profiles of Gly residues in U-^{13}C, >50% ^2H labeled proteins. ^1H, ^{13}C, ^{15}N and ^2H RF pulses denoted by narrow and wide *rectangular bars* correspond to flip angles of 90° and 180°, respectively. With the exception of the ^1H refocusing pulses during the CPMG period and the two flanking 90° pulses that are applied with a field strength of 25 kHz, all other rectangular pulses make use of the highest available power (32, 18, 6 and 2 kHz for ^1H, ^{13}C, ^{15}N and ^2H, respectively). ^1H, ^{13}C, ^{15}N and ^2H carriers are placed at 4.75, 45, 118 and 4.75 ppm, respectively. The shaped ^{13}C pulses (3 ms, at both 600 and 800 MHz) are of the REBURP variety (Geen and Freeman 1991) and are centered at 45 ppm. Carbonyl decoupling is performed using the WURST2 decoupling scheme (Kupce and Freeman 1996) centered at 175 ppm with a bandwidth of 12 ppm. ^2H WALTZ-16 decoupling (Shaka et al. 1983) is achieved with a field strength of 650 Hz. All pulses are applied with phase x unless indicated otherwise. An eight step phase cycle is carried out with $\phi1 = 4(x), 4(-x)$, $\phi2 = 2(x), 2(-x)$, $\phi3 = (x, -x)$ and receiver $= x, 2(-x), x$. Quadrature detection in F_1 is achieved by incrementing phase $\phi2$ in a STATES-TPPI manner (Marion et al. 1989). The delays τ_a and τ_{eq} are set to 1.785 and 3 ms, respectively. N is any integer. The ^1H pulses shown in the *dashed boxes* are applied to generate ^1H–^{13}C MQ coherence, as opposed to ^{13}C SQ coherence, during t_1. Gradients are applied along the z axis with the following strengths and durations (G/cm; ms): g1 = (5; 1), g2 = (8; 0.1), g3 = (4; 0.1), g4 = (−12; 1), g5 = (−15; 0.3), g6 = (−8; 0.1) and g7 = (14; 0.1). Pulse sequence code is available as supporting material

peak intensities quantified using the program FuDA (http://pound.med.utoronto.ca/software.html). Peak intensities (I) were converted into effective relaxation rates according to the relation

$$R_{2,\mathrm{eff}} = \frac{-1}{T_{\mathrm{relax}}} \ln\left(\frac{I(\nu_{\mathrm{CPMG}})}{I(0)}\right), \quad (1)$$

where $I(\nu_{\mathrm{CPMG}})$ and $I(0)$ are the signal intensities in the presence and absence of the CPMG element, respectively (Mulder et al. 2001b). Relaxation dispersion curves were analyzed using the program CATIA (http://pound.med.utoronto.ca/software). $^1H^\alpha$ and $^{13}C^\alpha$ relaxation dispersion profiles of Gly were combined with $^1H^\alpha$ dispersions obtained for non-Gly residues recorded using a previously published sequence (Lundstrom et al. 2009) with all profiles fit simultaneously to a two-state model of exchange. We have included $^1H^\alpha$ profiles from all residues in the fit to increase the number of dispersions so that accurate estimates of the population of the excited state, p_b (2.7 ± 0.1%) and the exchange rate, k_{ex} (830 ± 50 s^{-1}), could be obtained. $^{13}C^\alpha$ dispersion profiles from both of the CHD isotopomers of each Gly residue were fit assuming the same difference in chemical shift between the ground and excited states ($\Delta\varpi$).

Results and discussion

Probing exchange with Gly $^1H^\alpha$ spins

Recently we have presented a labeling scheme and associated pulse sequences for measuring $^1H^\alpha$ CPMG relaxation dispersion profiles for all residues in a protein with the exception of Gly (Lundstrom et al. 2009). For these experiments we have made use of a labeling protocol in which proteins are enriched to >50% in ^2H (50% enrichment at the C^α position) and 100% in ^{13}C that eliminates many of the homonuclear scalar coupling pathways of magnetization transfer that are otherwise operative during the CPMG element. The effects of residual ^1H–^1H couplings were minimized using a filter that refocuses scalar coupling evolution in the case of a homonuclear spin-pair. Here we use the same labeling strategy that in the case of Gly produces four equally populated isotopomers, CH_2, CHD, CDH and CD_2. Of the three proton containing groups that in principle could be exploited for measuring $^1H^\alpha$ relaxation dispersion profiles the CH_2 moiety is problematic because of the large $^1H^\alpha$–$^1H^\alpha$ scalar coupling; the resulting evolution of $^1H^\alpha$ magnetization due to this interaction produces artificial dispersion profiles that depend on ν_{CPMG}, even in cases where exchange is not present (Lundstrom et al. 2009). By contrast, both CHD and CDH moieties are well suited as probes since the troublesome $^1H^\alpha$ couplings are removed and replacing one of the two protons with a deuteron leads to increased transverse relaxation times for the remaining proton (Kushlan and Lemaster 1993).

The pulse sequence for measuring $^1H^\alpha$ CPMG relaxation dispersion profiles in proteins that are U-^{13}C, >50% ^2H labeled is shown in Fig. 1. The experiment follows closely the ^1HN CPMG sequence of Ishima and Torchia (2003) with a number of differences that are specific to the labeling scheme chosen. The flow of magnetization can be summarized briefly by

$$\begin{aligned} {}^1H_i^\alpha \xrightarrow{\mathrm{PurgeCH_2}} {}^{13}C^\alpha(t_1) &\rightarrow {}^1H_i^\alpha(\mathrm{CPMG}) \\ &\rightarrow {}^1H_i^\alpha(t_2), \quad i = 1, 2. \end{aligned} \quad (2)$$

^1H longitudinal magnetization at point a in the scheme is converted to $^1H^\alpha$–$^{13}C^\alpha$ multiple-quantum coherence at point b, $2H_X^iC_Y$, where H_X (C_Y) corresponds to the X (Y)-component of proton (carbon) magnetization. During the subsequent interval of duration $2\tau_a = 1/2J_{\mathrm{HC}}$, where J_{HC} is the one-bond ^1H–^{13}C scalar coupling constant, coherence originating on CH_2 isotopomers evolves to produce $4H_X^iH_Z^iC_X$ that is subsequently dephased by the gradient g4 after point c. By contrast coherences originating from CHD/CDH isotopomers are converted to $2H_Z^iC_Z$ after the simultaneous $^{13}C/^1H$ pulses at point c and this longitudinal order is immune to the action of gradient g4. Thus, only the 'singly protonated' glycine residues give rise to signals in correlation maps, eliminating the problem with $^1H^\alpha$–$^1H^\alpha$ scalar coupling and resulting in significant improvements in spectral resolution, as discussed below. Immediately following the purge element $^{13}C^\alpha$ chemical shift is recorded during t_1 that is then followed by a constant-time ^1H CPMG period. The ^1H π pulse in the center of this element leads to a net refocusing of artifacts that would otherwise result from pulse imperfections and off-resonance effects, as described previously (Hansen et al. 2008a). Finally, $^1H^\alpha$ magnetization is detected during t_2, so that 2D (^{13}C, ^1H) data sets are produced with peak intensities that vary as a function of $\nu_{\mathrm{CPMG}} = N/T_{\mathrm{relax}}$ (in the case of chemical exchange).

We have chosen to place the CPMG element after the t_1 period, despite the fact that it is then not possible to preserve both cosine and sine t_1 evolution components that is desirable for sensitivity enhancement (Palmer et al. 1991). As described by Ishima and Torchia the relaxation properties of spin-locked ^1H magnetization are more favorable using this approach since the decay of signal is given by the auto-relaxation rate as opposed to the sum of auto- and cross-rates that are of the same sign in the case of transverse relaxation (Ishima and Torchia 2003; Ishima et al. 1998). Further since the initial magnetization state at the start of the CPMG interval is anti-phase $^1H^\alpha$ with

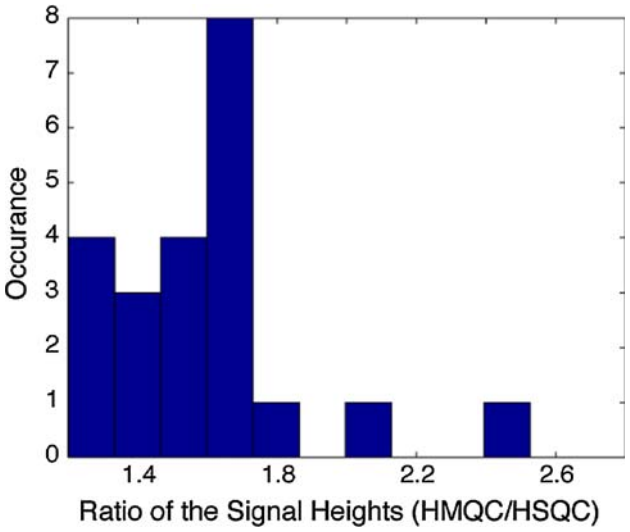

Fig. 2 Spectra recorded with ^{1}H–^{13}C MQ evolution (pulse scheme of Fig. 1) have significant improvements in sensitivity over those recorded with ^{13}C SQ evolution. Distribution of the ratio of Gly $^{1}H^{\alpha}$–$^{13}C^{\alpha}$ peak intensities in 2D spectra of T4 L99A, 25°C, 600 MHz, recorded with MQ and SQ evolution during t_1 ($t_{1,\max} = 26.6$ ms). The improvement in sensitivity for MQ spectra is 1.6 ± 0.3

respect to the one-bond coupled $^{13}C^{\alpha}$ any cross-relaxation between proximal proton spins (H^i and H^k) will not produce observable signal since magnetization of the form $2H_Y^kC_Z^i$ is created where H^k and C^i are not coupled. Finally, it is worth mentioning that on average over the complete T_{relax} period equal amounts of in-phase and anti-phase $^{1}H^{\alpha}$ magnetization will in general not be present. This imbalance leads to a dependence of $R_{2,\text{eff}}$ on ν_{CPMG} that arises from the difference in relaxation rates of H_Y^k and $2H_Y^kC_Z^i$ (Loria et al. 1999) that is not corrected for in the analysis of our data. However, errors less than 1 s^{-1} from this effect are predicted, smaller than the uncertainties in the measurements.

^{1}H–^{13}C dipolar interactions lead to efficient relaxation of $^{1}H^{\alpha}$ or $^{13}C^{\alpha}$ magnetization in proteins (Bax et al. 1990). Relaxation loses in the scheme of Fig. 1 can be minimized by recording ^{13}C chemical shift (t_1) when the coherence of interest is of the ^{1}H–^{13}C multiple-quantum (MQ) variety as opposed to ^{13}C single-quantum (Grzesiek and Bax 1995), since in the former case there are no transverse relaxation contributions from the $^{1}H^{\alpha}$–$^{13}C^{\alpha}$ dipolar interaction that

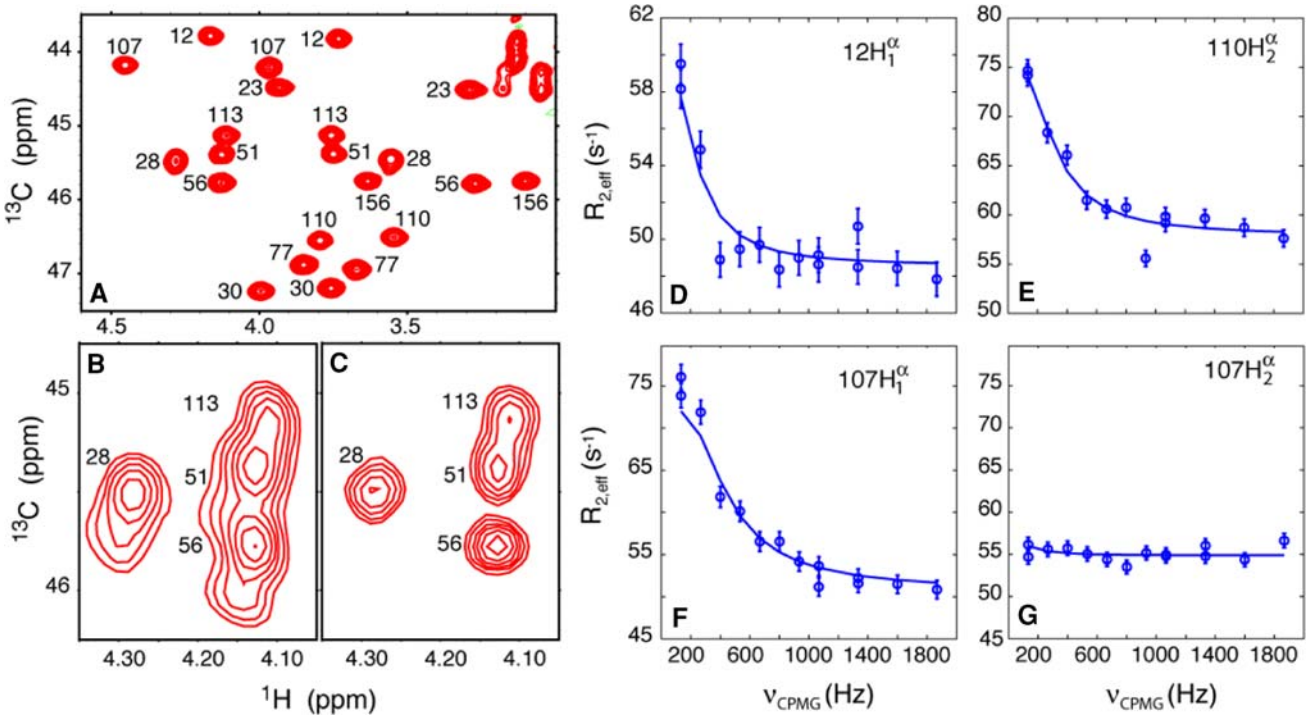

Fig. 3 Conformational exchange in T4 L99A studied via $^{1}H^{\alpha}$ CPMG relaxation dispersion. **a** Reference Gly $^{1}H^{\alpha}$–$^{13}C^{\alpha}$ 2D spectrum recorded on a sample of U-^{13}C, >50% ^{2}H T4 L99A, 25°C, 600 MHz, with the scheme of Fig. 1, $T_{\text{relax}} = 0$ ms. All of the expected 22 peaks (corresponding to Gly $H^{\alpha 1}$, $H^{\alpha 2}$) are well resolved and labeled according to their position in the primary sequence. Stereospecific assignments for the protons are not available. **b** Selected region of the $^{1}H^{\alpha}$–$^{13}C^{\alpha}$ spectrum recorded with the scheme of Fig. 1 but without the purge element. The peaks arising from Gly CH_2 groups can be seen as shoulders (*downfield*) on the main correlations derived from the ^{13}CHD isotopomer. **c** As in (**b**) but recorded with the purge element so that correlations from CH_2 groups are suppressed. **d**–**g** Gly $^{1}H^{\alpha}$ dispersions from selected residues (*circles*) along with best fits of the data to a two-state model of chemical exchange (*solid lines*), as described in "Materials and methods". Errors are indicated by *vertical bars*. Note that only one of the two protons of Gly 107 is sensitive to the chemical exchange process

scale with molecular correlation time (i.e., no J(0) contributions, where J(ω) is the spectral density function evaluated at ω) (Griffey and Redfield 1987; Roy et al. 1984). This is offset to some extent by transverse relaxation between $^1H^\alpha$ and proximal proton spins. However, in cases where the proton density is low, such as for Gly residues that lack a side-chain and where the protein is relatively highly deuterated as in the present sample, significant sensitivity benefits can be achieved. This is illustrated in Fig. 2 that plots ratios of signal intensities measured in spectra recorded where the coherences of interest during t_1 are of the MQ or SQ variety (net t_1 acquisition times of 26.6 ms). An average gain in sensitivity of a factor of 1.6 $\pm$ 0.3 is obtained using the MQ version of the experiment that is readily performed by inserting a pair of ^{1}H pulses that bracket the t_1 evolution time (indicated by dashes in Fig. 1) along with a proton π pulse in the middle of the t_1 period that refocuses the proton chemical shift evolution so that magnetization is labeled with only the $^{13}C^\alpha$ frequency during the t_1 period.

Figure 3a shows the 2D ^{13}C, ^{1}H Gly correlation map of T4 L99A, 600 MHz, 25°C recorded using the scheme of Fig. 1 with $T_{relax} = 0$. That the purge element is effective in suppressing signal originating from CH_2 moieties can be appreciated by comparison of spectra recorded without (Fig. 3b) and with (Fig. 3a, c) the purge. Figure 3b highlights the fact that signals from CH_2 and CHD moieties are in separate positions in spectra due to a deuterium isotope shift (Hansen 2000), effectively doubling the number of peaks in the 'non-purged' spectrum. Not surprisingly there are thus significant resolution advantages when signals from only CHD/CDH isotopomers are observed. Figure 3d–g show dispersion profiles measured at a number of sites in the protein, along with fits of the dispersion curves to a two-site model of chemical exchange (solid lines). As expected the large dispersions are localized to regions proximal to the cavity (Mulder et al. 2001a), with many of the $^1H^\alpha$ probes impervious to the exchange event.

A pulse scheme for measuring Gly $^{13}C^\alpha$ relaxation dispersion profiles

An ^{15}N relaxation dispersion experiment probing exchange involving AX_2/AMX spin systems in proteins has previously been proposed in the context of some of our earlier work involving T4 L99A where we focused on $^{15}NH_2$ groups of Asn and Gln (Mulder et al. 2001b). Although the experiments developed previously are equally applicable to $^{13}CH_2$ moieties of Gly residues, we have chosen to develop an alternative strategy here for a number of reasons. First, the ^{1}H–^{13}C dipolar interaction is a factor of two larger than for ^{1}H–^{15}N so that all things equal transverse relaxation rates of ^{13}C are approximately a factor of four larger than

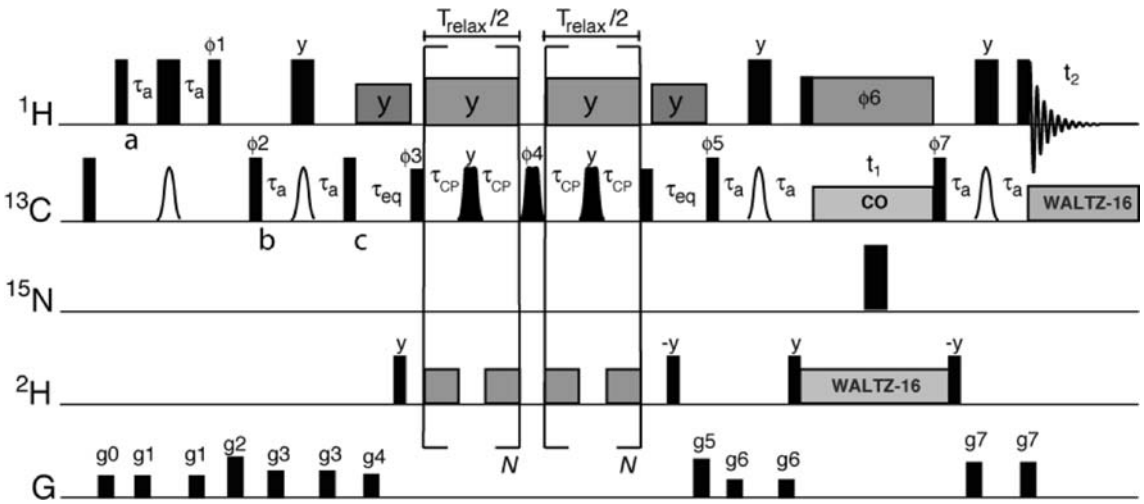

Fig. 4 Pulse sequence for recording $^{13}C^\alpha$ CPMG relaxation dispersion profiles of Gly residues in U-^{13}C, >50% ^{2}H labeled proteins. Many of the details of this pulse scheme are the same as for the $^1H^\alpha$ CPMG relaxation dispersion experiment and can be found in the legend to Fig. 1. The shaped pulses (450 ms, 600 MHz) during the CPMG interval are derivates of REBURP pulses that have been described previously (Lundstrom et al. 2008). The 90° pulses on either side of the CPMG period were applied at a field strength equal to the maximum used for the shaped pulses. The phase cycle is: $\phi1 = 4(y),4(-y)$, $\phi2 = 2(y),2(-y)$, $\phi3 = 4(x),4(-x)$, $\phi4 = 8(x),8(-x)$, $\phi5 = (y, -y)$, $\phi6 = (8y, 8-y)$, $\phi7 = (x)$ and receiver = x, $2(-x)$, x. Quadrature detection in F_1 was achieved by STATES phase incrimination of phase $\phi5$ (States et al. 1982). The phase $\phi7$ was inverted with each successive complex t_1 point (Marion et al. 1989). ^{1}H decoupling during the CPMG element was achieved as described previously (Hansen et al. 2008a; Vallurupalli et al. 2007b) and in the text using a maximum CW field of 13.3 kHz. For $N = 0$ a ^{1}H CW pulse of duration T_{relax} is applied after t_2 so that the amount of sample heating is independent of N. ^{2}H decoupling during T_{relax} made use of a 675 Hz field, with a scheme described in the text. ^{1}H purge pulses before and after the CPMG period were applied at a field of 9.4 kHz. Gradients, applied along the z axis had the following strength and durations (G/cm:ms):g0 = (12:1), g1 = (13:0.16), g2 = (23:1.5), g3 = (15:0.16), g4 = (12:1), g5 = (20:1.5), g6 = (4:1) and g7 = (17:0.150)

the corresponding rates for ^{15}N. The large R_2 rates for $^{13}C^{\alpha}$ of Gly that is coupled to a pair of protons (typically on the order of 100 s^{-1} for L99A T4 at 25°C) is prohibitive for measuring chemical exchange, especially in cases where only small contributions to R_2 from exchange are generated. In principle, it is possible to make use of TROSY based schemes for $^{13}CH_2$ groups that exploit the partial cancellation of dipolar fields, as has recently been

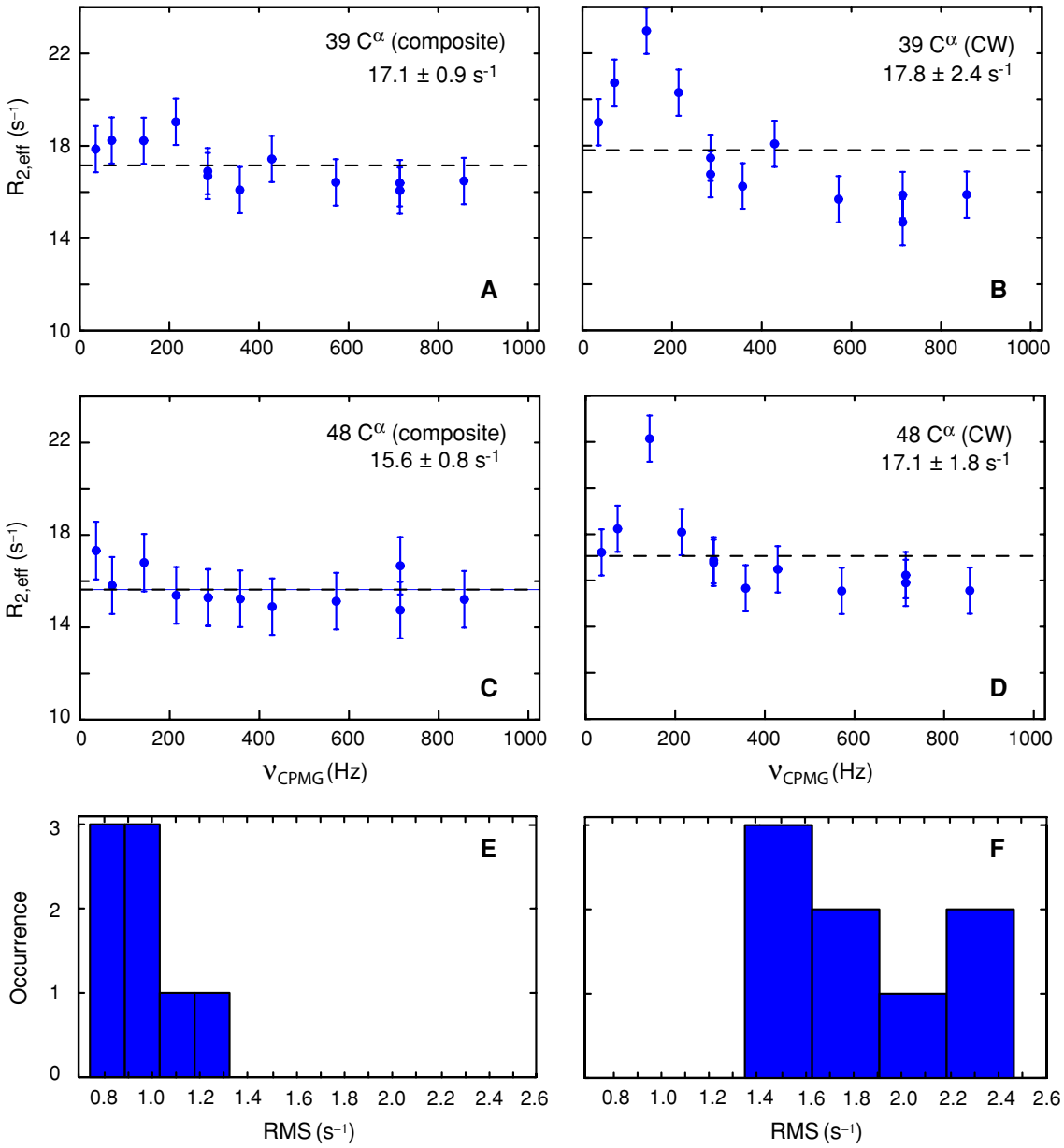

Fig. 5 **a–d** $^{13}C^{\alpha}$ CPMG relaxation dispersion profiles of Gly 39 and 48 in a U-^{13}C, 50% ^{2}H labeled Abp1p SH3 domain recorded with the pulse scheme of Fig. 4, 25°C, 500 MHz. Note that this protein does not undergo conformational exchange on the millisecond time-scale and flat dispersion profiles are therefore expected. Profiles from only one of the two isotopomers of each Gly are shown. **a** and **c** show dispersion curves recorded using the ^{2}H decoupling scheme described in the text ('composite decoupling') where different decoupling elements are applied depending on the duration of τ_{CP}. The corresponding profiles, with an integral number of ^{2}H 180° pulses in each τ_{CP} element, using the same approach as for ^{1}H decoupling described above and in Vallurupalli et al. 2007b, but with a much lower field, are shown in **b** and **d**. In all cases ^{1}H decoupling with an average field of 14 kHz was employed (*see text*). Values of $\langle R_{2eff} \rangle \pm$ RMSD are shown in each panel; elevated $R_{2,eff}$ values at $\nu_{CPMG} \sim 175$ Hz in panels **b** and **d** indicate that the ^{2}H CW scheme is not decoupling properly. Panels **e** and **f** show histograms of the distribution of RMSD values from fits of Gly dispersions recorded with the composite decoupling approach and using the method of Vallurupalli et al. (2007b), respectively. A significant improvement is noted with the ^{2}H composite decoupling scheme with RMSD values of a factor of two smaller than those for CW decoupling (average RMSD of 1.0 vs. 1.9)

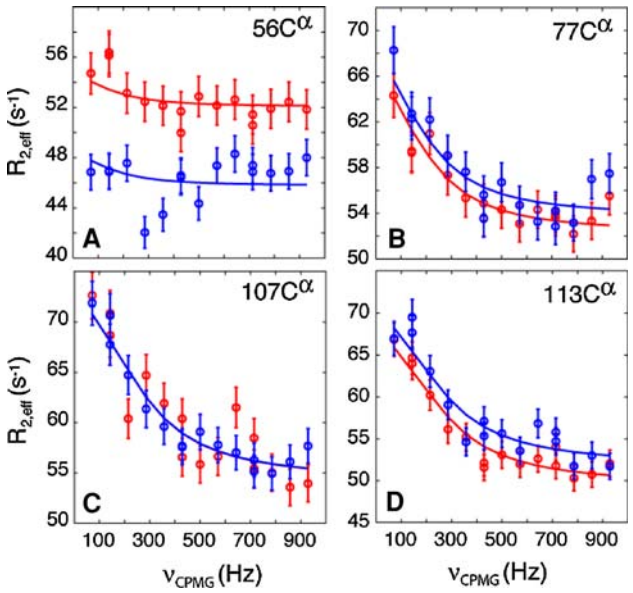

Fig. 6 Gly $^{13}C^{\alpha}$ relaxation dispersion profiles recorded on a 100%^{13}C, >50% ^{2}H T4 L99A sample, 25°C, 600 MHz, with the pulse sequence of Fig. 4. *Red* and *blue curves* derive from each of the two Gly isotopmers (CHD and CDH) that report on exchange involving the same $^{13}C^{\alpha}$ spin

demonstrated for applications that are unrelated to those considered presently (Miclet et al. 2004). Here we have chosen an alternative approach that uses samples that have already been prepared for recording $^{1}H^{\alpha}$ CPMG relaxation dispersion profiles in which proteins are U-^{13}C and >50% deuterated (Lundstrom et al. 2009). As in the Gly $^{1}H^{\alpha}$ CPMG dispersion experiment described above CHD/CDH moieties are selected for the $^{13}C^{\alpha}$ measurements that have significantly improved relaxation properties over CH_2 groups.

Figure 4 illustrates the pulse scheme that has been developed for recording Gly $^{13}C^{\alpha}$ relaxation dispersion profiles and in what follows a brief description of some of its salient features is provided. Longitudinal ^{1}H magnetization originating on CHD/CDH methylenes at point *a* is transferred into ^{13}C *Z*-magnetization at point *c* through a refocused INEPT scheme (Burum and Ernst 1980). By contrast, magnetization transfer from $^{13}CH_2$ groups is suppressed because anti-phase ^{13}C magnetization is not refocused by the element between *b* and *c* for a carbon spin attached to a pair of protons. Thus immediately after point *c* magnetization from $^{13}CH_2$ moieties is of the form $2C_XH_Z^i$ that is dephased by gradient g4. During the subsequent constant-time ^{13}C CPMG element evolution of magnetization due to both ^{1}H–^{13}C and ^{2}H–^{13}C one-bond scalar couplings is suppressed by the action of the simultaneous ^{1}H and ^{2}H decoupling fields. Ensuring that ^{13}C magnetization is in-phase throughout this period is important for a number of reasons. First, the transverse relaxation of $^{13}C^{\alpha}$ in this case does not depend on dipolar interactions between the attached $^{1}H^{\alpha}$ and proximal protons. In the absence of ^{1}H decoupling, however, a CPMG element must be used that ensures that $^{13}C^{\alpha}$ magnetization is equally distributed between in-phase and anti-phase components (on average) effectively elevating the transverse relaxation rate by an amount $1/2R_{HH}$, where R_{HH} is the selective $^{1}H^{\alpha}$ longitudinal relaxation rate (Loria et al. 1999). Second, ^{2}H decoupling prevents the accumulation of magnetization of the form $2C_XD_Z$, $2C_YD_Z$ that would decay rapidly due to the efficient relaxation of the deuteron that can be on the order of several ms in the case of moderately sized proteins. At the completion of the CPMG element, $^{1}H^{\alpha}$–$^{13}C^{\alpha}$ MQ coherence is created so that its favorable relaxation properties can be exploited during the t_1 period where $^{13}C^{\alpha}$ chemical shift evolution is recorded prior to the subsequent transfer of magnetization to $^{1}H^{\alpha}$ for detection. The magnetization transfer scheme is thus summarized as

$$^{1}H_i^{\alpha} \xrightarrow{\text{PurgeCH}_2} {}^{13}C^{\alpha}(\text{CPMG}) \rightarrow {}^{13}C^{\alpha}(t_1) \rightarrow {}^{1}H_i^{\alpha}(t_2), \quad i = 1, 2 \tag{3}$$

As described above the ^{1}H and ^{2}H decoupling elements that preserve in-phase $^{13}C^{\alpha}$ magnetization during the course of the CPMG pulse train are critical components of the scheme of Fig. 4. Care must be taken to ensure that application of the decoupling fields does not interfere with the refocusing properties of the CPMG pulses (Hansen et al. 2008a; Vallurupalli et al. 2007b). In the case of ^{1}H decoupling we make use of a scheme in which the ^{1}H continuous wave (CW) field strength, ν_{CW}, is adjusted for each ν_{CPMG} value in such a way so as to ensure that an integral number of decoupling pulses is present in every τ_{CP} element ($2\tau_{CP}$ is the time between the centers of successive $^{13}C^{\alpha}$ refocusing pulses). This is accomplished by choosing $\nu_{CW} = 2\,k\nu_{CPMG}$ where k is an integer, as described in detail previously (Hansen et al. 2008a; Vallurupalli et al. 2007b). Typically an average ^{1}H CW field of approximately 15 kHz is employed with variations of not more than 11% over the range of ν_{CPMG} values chosen. In the case of ^{2}H decoupling there is a much more strict technical limitation on the field strength that can be used. Here we have chosen to employ a strategy in which the nature of the decoupling scheme depends on the duration of τ_{CP}. For $\tau_{CP} \leq pw_D^{180}$, where pw_D^{180} is the ^{2}H 180° pulse width, no decoupling is employed. For the cases where $pw_D^{180} < \tau_{CP} \leq 2pw_D^{180}$, $2pw_D^{180} < \tau_{CP} \leq 3pw_D^{180}$ pulses of the form 180°_X and $90^{\circ}_X - 180^{\circ}_Y - 90^{\circ}_X$ are applied, respectively, centered in the τ_{CP} interval. For $3pw_D^{180} < \tau_{CP} \leq 12pw_D^{180}$ the maximum number of composite pulses, $90^{\circ}_X - 180^{\circ}_{-X} - 270^{\circ}_X$, that can be fit into the τ_{CP} duration is used. Finally, for $\tau_{CP} > 12pw_D^{180}$ WALTZ-4 decoupling (Shaka et al. 1983) is employed that has a length of

$12pw_D^{180}$ per cycle. An integral number of cycles is not necessarily applied but an integral number of 180° pulses always is, again with the decoupling centered in the τ_{CP} interval (pulse sequence code available upon request). The effectiveness of the ^{2}H decoupling scheme was tested by recording spectra using the pulse sequence of Fig. 4 on a sample of a U-^{13}C, 50% ^{2}H labeled Abp1p SH3 domain that does not undergo millisecond time-scale exchange so that flat dispersion profiles are expected (Vallurupalli et al. 2007a). We have chosen this small protein as a test sample since significantly higher sensitivity spectra can be recorded relative to T4 L99A. Figure 5 compares a pair of dispersion profiles recorded on the Apbp1 SH3 domain obtained with the decoupling scheme described above (referred to as 'composite') and with decoupling that involves the application of 180° pulses (referred to as 'CW') in which the field strength is adjusted to ensure use of an integral number of pulses in each τ_{CP} period as for ^{1}H. Also shown are histograms of RMSD values obtained from fits of all Gly dispersion profiles generated with the two different ^{2}H decoupling approaches, where RMSD $= \sqrt{\mathrm{ND}^{-1}\sum_i \{R^i_{2,\mathrm{eff}}(\nu_{\mathrm{CPMG},i}) - k\}^2}$, $R^i_{2,\mathrm{eff}}$ is the effective transverse relaxation rate at CPMG frequency $\nu_{\mathrm{CPMG},i}$, $k = \langle R_{2,\mathrm{eff}}(\nu_{\mathrm{CPMG}})\rangle$ and ND is the number of data points in the dispersion profile. It is clear that the composite scheme is preferred, although not perfect. Improved decoupling could be achieved with higher fields although this is unlikely to be an option using the current generation of probes.

$^{13}C^{\alpha}$ dispersion profiles for Gly 56, 77, 107 and 113 of T4 L99A are illustrated in Fig. 6 (600 MHz, 25°C). Because cross-peaks from both CHD and CDH

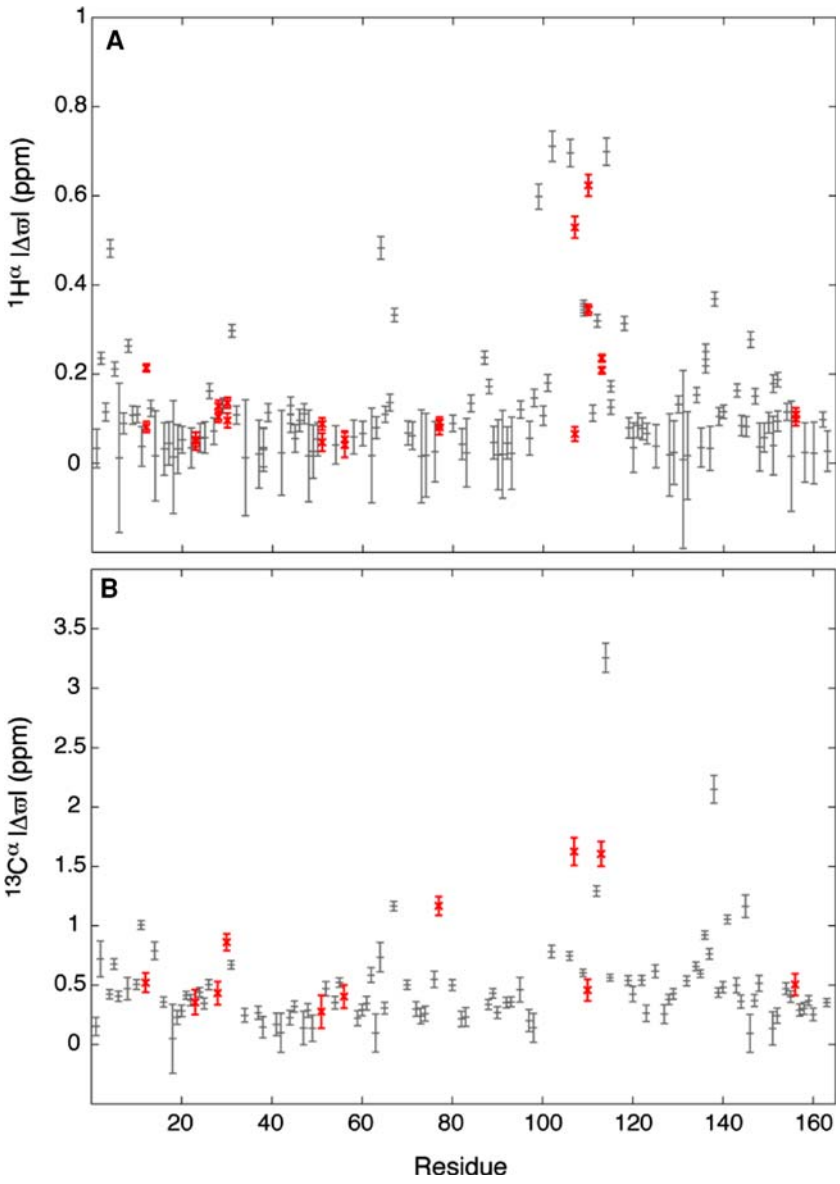

Fig. 7 Absolute values of the changes in $^1H^{\alpha}$ (**a**) and $^{13}C^{\alpha}$ (**b**) chemical shifts (ppm), $|\Delta\varpi|$, between ground and excited states of T4 L99A, showing that the major conformational changes associated with the exchange occur in a region that surrounds the cavity. Values of Gly $|\Delta\varpi|$ are shown in red; the $|\Delta\varpi|$ values for non-Gly residues (shown in *gray*) were measured as described previously for $^{13}C^{\alpha}$ (Hansen et al. 2008a, b, c, d) and $^1H^{\alpha}$ (Lundstrom et al. 2009)

isotopomers are observed in spectra it is possible to probe exchange at each $^{13}C^{\alpha}$ position twice, with pairs of dispersion profiles obtained for each Gly (Fig. 6). Notably, the ^{13}C relaxation properties of the CHD/CDH isotopomers can be distinct, as illustrated for Gly 56, that may reflect differences in the orientation of the ^{1}H–^{13}C bond vectors with respect to the diffusion frame of the protein. Several of the experimental data points (circles) are clearly removed from the solid lines corresponding to the global fits of the dispersion data, even when experimental errors are taken into account, likely reflecting the imperfections in ^{2}H decoupling even with the improved scheme described in the text. Only a few of the $^{1}H^{\alpha}$ and $^{13}C^{\alpha}$ probes of the eleven glycine residues in T4 L99A show significant changes in chemical shifts between the ground and excited states, Fig. 7. The residues that sense the chemical exchange process include Gly 77, 107, 110 and 113 that are localized to a small region in and around helix F that is proximal to the cavity and that likely participates in an 'opening' event that allows access to ligands. The fact that only a few of the Gly residues report on the exchange event is not surprising given that both $^{1}H^{\alpha}$ and $^{13}C^{\alpha}$ chemical shifts are sensitive to secondary structural changes that are expected in only a relatively small region of the protein (Mulder et al. 2001a; Skrynnikov et al. 2002).

In summary, glycine-specific $^{1}H^{\alpha}$ and $^{13}C^{\alpha}$ relaxation dispersion experiments have been presented for the characterization of millisecond timescale conformational exchange processes in proteins. The experiments exploit a recently introduced labeling scheme that has been proposed for the measurement of $^{1}H^{\alpha}$ dispersion profiles of non-Gly residues in which proteins are prepared with U-^{13}C, >50% ^{2}H labeling (Lundstrom et al. 2009). Gly ^{13}CHD isotopomers are selected which, as described in the text, have distinct advantages over $^{13}CH_2$ moieties which would otherwise be available as probes in fully protonated protein samples. It is well known that Gly can adopt a wide range of conformations in proteins (Ramakrishnan and Ramachandran 1965) and the determination of Gly backbone (Φ, Ψ) dihedral angles is thus an important step in structural studies. The methods presented here enable measurement of Gly $^{1}H^{\alpha}$ and $^{13}C^{\alpha}$ chemical shifts in the excited states of protein molecules from which torsion angles can be derived (Cornilescu et al. 1999); as such they will be a powerful addition to the growing set of experiments that characterize the structural features of invisible, yet functionally important conformations of biomolecules.

Acknowledgments This work was supported by funds from the Canadian Institutes of Health Research (CIHR) in the form of a research grant to LEK and postdoctoral fellowships to DFH and PL (Protein Folding Training Grant). LEK holds a Canada Research Chair in Biochemistry.

References

Austin RH, Beeson KW, Eisenstein L, Frauenfelder H, Gunsalus IC (1975) Dynamics of ligand binding to myoglobin. Biochemistry 14:5355–5373

Bax A, Ikura M, Kay LE, Torchia DA, Tschudin R (1990) Comparison of different modes of 2-dimensional reverse-correlation NMR for the study of proteins. J Magn Reson 86:304–318

Boehr DD, McElheny D, Dyson HJ, Wright PE (2006) The dynamic energy landscape of dihydrofolate reductase catalysis. Science 313:1638–1642

Burum DP, Ernst RR (1980) Net polarization transfer via a J-ordered state for signal enhancement of low-sensitivity nuclei. J Magn Reson 39:163–168

Carr HY, Purcell EM (1954) Effects of diffusion on free precession in nuclear magnetic resonance experiments. Phys Rev 94:630–638

Cornilescu G, Delaglio F, Bax A (1999) Protein backbone angle restraints from searching a database for chemical shift and sequence homology. J Biomol NMR 13:289–302

Delaglio F, Grzesiek S, Vuister GW, Zhu G, Pfeifer J, Bax A (1995) NMRPipe: A multidimensional spectral processing system based on UNIX pipes. J Biomol NMR 6:277–293

Eriksson AE, Baase WA, Wozniak JA, Matthews BW (1992) A cavity-containing mutant of T4 lysozyme is stabilized by buried benzene. Nature 355:371–373

Feher VA, Baldwin EP, Dahlquist FW (1996) Access of ligands to cavities within the core of a protein is rapid. Nat Struct Biol 3:516–521

Geen H, Freeman R (1991) Band-selective radiofrequency pulses. J Magn Reson 93:93–141

Goddard TD, Kneller DG. SPARKY 3. University of California, San Francisco

Grey MJ, Wang C, Palmer AG III (2003) Disulfide bond isomerization in basic pancreatic trypsin inhibitor: multisite chemical exchange quantified by CPMG relaxation dispersion and chemical shift modeling. J Am Chem Soc 125:14324–14335

Grey MJ, Tang Y, Alexov E, McKnight CJ, Raleigh DP, Palmer AG III (2006) Characterizing a partially folded intermediate of the villin headpiece domain under non-denaturing conditions: contribution of His41 to the pH-dependent stability of the N-terminal subdomain. J Mol Biol 355:1078–1094

Griffey RH, Redfield AG (1987) Proton-detected heteronuclear edited and correlated nuclear magnetic resonance and nuclear overhauser effect in solution. Q Rev Biophys 19:51–82

Grzesiek S, Bax A (1995) Spin-locked multiple quantum coherence for signal enhancement in heteronuclear multidimensional NMR experiments. J Biomol NMR 6:335–339

Hansen PE (2000) Isotope effects on chemical shifts of proteins and peptides. Magn Reson Chem 38:1–10

Hansen DF, Vallurupalli P, Kay LE (2008a) An improved 15N relaxation dispersion experiment for the measurement of millisecond time-scale dynamics in proteins. J Phys Chem B 112:5898–5904

Hansen DF, Vallurupalli P, Kay LE (2008b) Quantifying two-bond 1HN-13CO and one-bond 1H(alpha)-13C(alpha) dipolar couplings of invisible protein states by spin-state selective relaxation dispersion NMR spectroscopy. J Am Chem Soc 130:8397–8405

Hansen DF, Vallurupalli P, Kay LE (2008c) Using relaxation dispersion NMR spectroscopy to determine structures of excited, invisible protein states. J Biomol NMR 41:113–120

Hansen DF, Vallurupalli P, Lundstrom P, Neudecker P, Kay LE (2008d) Probing chemical shifts of invisible states of proteins with relaxation dispersion NMR spectroscopy: How well can we do? J Am Chem Soc 130:2667–2675

Henzler-Wildman KA, Thai V, Lei M, Ott M, Wolf-Watz M, Fenn T, Pozharski E, Wilson MA, Petsko GA, Karplus M, Hubner CG, Kern D (2007) Intrinsic motions along an enzymatic reaction trajectory. Nature 450:838–844

Igumenova TI, Brath U, Akke M, Palmer AG III (2007) Characterization of chemical exchange using residual dipolar coupling. J Am Chem Soc 129:13396–13397

Ishima R, Torchia DA (2003) Extending the range of amide proton relaxation dispersion experiments in proteins using a constant-time relaxation-compensated CPMG approach. J Biomol NMR 25:243–248

Ishima R, Wingfield PT, Stahl SJ, Kaufman JD, Torchia DA (1998) Using amide H-1 and N-15 transverse relaxation to detect millisecond time-scale motions in perdeuterated proteins: application to HIV-1 protease. J Am Chem Soc 120:10534–10542

Karplus M (2000) Aspects of protein reaction dynamics: deviations from simple behavior. J Phys Chem B 104:11–27

Karplus M, Kuriyan J (2005) Molecular dynamics and protein function. Proc Natl Acad Sci USA 102:6679–6685

Korzhnev DM, Kay LE (2008) Probing invisible, low-populated states of protein molecules by relaxation dispersion NMR spectroscopy: an application to protein folding. Acc Chem Res 41:442–451

Korzhnev DM, Salvatella X, Vendruscolo M, Di Nardo AA, Davidson AR, Dobson CM, Kay LE (2004) Low-populated folding intermediates of Fyn SH3 characterized by relaxation dispersion NMR. Nature 430:586–590

Kupce E, Freeman R (1996) Optimized adiabatic pulses for wideband spin inversion. J Magn Reson A 118:299–303

Kushlan DM, Lemaster DM (1993) Resolution and sensitivity enhancement of heteronuclear correlation for methylene resonances via H-2-enrichment and decoupling. J Biomol NMR 3:701–708

Loria JP, Rance M, Palmer AG (1999) A relaxation-compensated Carr-Purcell-Meiboom-Gill sequence for characterizing chemical exchange by NMR spectroscopy. J Am Chem Soc 121:2331–2332

Lundstrom P, Hansen DF, Kay LE (2008) Measurement of carbonyl chemical shifts of excited protein states by relaxation dispersion NMR spectroscopy: comparison between uniformly and selectively (13)C labeled samples. J Biomol NMR 42:35–47

Lundstrom P, Hansen DF, Vallurupalli P, Kay LE (2009) Accurate measurement of alpha proton chemical shifts of excited protein states by relaxation dispersion NMR spectroscopy. J Am Chem Soc 131:1915–1926

Marion D, Ikura M, Tschudin R, Bax A (1989) Rapid recording of 2D NMR spectra without phase cycling. Application to the study of hydrogen exchange in proteins. J Magn Reson 85:393–399

Meiboom S, Gill D (1958) Modified spin-echo method for measuring nuclear relaxation times. Rev Sci Instrum 29:688–691

Miclet E, Williams DC, Clore GM, Bryce DL, Boisbouvier J, Bax A (2004) Relaxation-optimized NMR spectroscopy of methylene groups in proteins and nucleic acids. J Am Chem Soc 126:10560–10570

Mittermaier A, Kay LE (2006) New tools provide new insights in NMR studies of protein dynamics. Science 312:224–228

Mulder FA, Hon B, Muhandiram DR, Dahlquist FW, Kay LE (2000) Flexibility and ligand exchange in a buried cavity mutant of T4 lysozyme studied by multinuclear NMR. Biochemistry 39:12614–12622

Mulder FA, Mittermaier A, Hon B, Dahlquist FW, Kay LE (2001a) Studying excited states of proteins by NMR spectroscopy. Nat Struct Biol 8:932–935

Mulder FA, Skrynnikov NR, Hon B, Dahlquist FW, Kay LE (2001b) Measurement of slow (micros-ms) time scale dynamics in protein side chains by (15)N relaxation dispersion NMR spectroscopy: application to Asn and Gln residues in a cavity mutant of T4 lysozyme. J Am Chem Soc 123:967–975

Palmer AG (2004) NMR characterization of the dynamics of biomacromolecules. Chem Rev 104:3623–3640

Palmer AG, Cavanagh J, Wright PE, Rance M (1991) Sensitivity improvement in proton-detected 2-dimensional heteronuclear correlation Nmr-spectroscopy. J Magn Reson 93:151–170

Palmer AG III, Kroenke CD, Loria JP (2001) Nuclear magnetic resonance methods for quantifying microsecond-to-millisecond motions in biological macromolecules. Methods Enzymol 339:204–238

Ramakrishnan C, Ramachandran GN (1965) Stereochemical criteria for polypeptide and protein chain conformations.2. Allowed conformations for a pair of peptide units. Biophys J 5:909–933

Roy S, Papastavros MZ, Sanchez V, Redfield AG (1984) Nitrogen-15-labeled yeast tRNAPhe: double and two-dimensional heteronuclear NMR of guanosine and uracil ring NH groups. Biochemistry 23:4395–4400

Shaka AJ, Keeler J, Frenkiel T, Freeman R (1983) An improved sequence for broad-band decoupling-Waltz-16. J Magn Reson 52:335–338

Skrynnikov NR, Dahlquist FW, Kay LE (2002) Reconstructing NMR spectra of "invisible" excited protein states using HSQC and HMQC experiments. J Am Chem Soc 124:12352–12360

States DJ, Haberkorn RA, Ruben DJ (1982) A two-dimensional nuclear overhauser experiment with pure absorption phase in 4 quadrants. J Magn Reson 48:286–292

Sugase K, Dyson HJ, Wright PE (2007) Mechanism of coupled folding and binding of an intrinsically disordered protein. Nature 447:1021–1025

Vallurupalli P, Kay LE (2006) Complementarity of ensemble and single-molecule measures of protein motion: a relaxation dispersion NMR study of an enzyme complex. Proc Natl Acad Sci USA 103:11910–11915

Vallurupalli P, Hansen DF, Stollar E, Meirovitch E, Kay LE (2007a) Measurement of bond vector orientations in invisible excited states of proteins. Proc Natl Acad Sci USA 104:18473–18477

Vallurupalli P, Scott L, Williamson JR, Kay LE (2007b) Strong coupling effects during X-pulse CPMG experiments recorded on heteronuclear ABX spin systems: artifacts and a simple solution. J Biomol NMR 38:41–46

Vallurupalli P, Hansen DF, Kay LE (2008a) Probing structure in invisible protein states with anisotropic NMR chemical shifts. J Am Chem Soc 130:2734–2735

Vallurupalli P, Hansen DF, Kay LE (2008b) Structures of invisible, excited protein states by relaxation dispersion NMR spectroscopy. Proc Natl Acad Sci USA 105:11766–11771

Watt ED, Shimada H, Kovrigin EL, Loria JP (2007) The mechanism of rate-limiting motions in enzyme function. Proc Natl Acad Sci USA 104:11981–11986